1 **Measurement report: Distinct Emissions and Volatility Distribution of Intermediate**

2 **Volatility Organic Compounds from on-road Chinese Gasoline Vehicle: Implication of**

3 **High Secondary Organic Aerosol Formation Potential**

4 Rongzhi Tang[1,#], Quanyang Lu[2,#], Song Guo[1,3,*], Hui Wang[1], Kai Song[1], Ying Yu[1], Rui Tan[1],

5 Kefan Liu[1], Ruizhe Shen[1], Shiyi Chen[1], Limin Zeng[1], Spiro D. Jorga[2], Zhou Zhang[4], Wenbin

6 Zhang[4], Shijin Shuai[4], Allen L. Robinson[2,*]

7 *1 State Key Joint Laboratory of Environmental Simulation and Pollution Control, College of*

8 *Environmental Sciences and Engineering, Peking University, Beijing, 100871, PR China*

9 *2 Department of Mechanical Engineering and Center for Atmospheric Particle Studies, Carnegie*

10 *Mellon University, 5000 Forbes Avenue, Pittsburgh, Pennsylvania 15213, United States*

11 *3 International Joint Laboratory for Regional Pollution Control, Ministry of Education, Beijing,*

12 *100816, PR China*

13 *4 State Key Laboratory of Automotive Safety and Energy, School of Vehicle and Mobility,Tsinghua*

14 *University, Beijing, 100084, PR China*

15 Correspondence to: S. Guo songguo@pku.edu.cn, A. Robinson:alr@andrew.cmu.edu

16 [#]These authors contribute equally to this work

18   **Abstract**

19   In the present work, we performed chassis dynamometer experiments to

20   investigate the emissions and secondary organic aerosol (SOA) formation potential of

21   intermediate volatility organic compounds (IVOCs) from an on-road Chinese gasoline

22   vehicle. High IVOCs emission factors (EFs) and distinct volatility distribution were

23   recognized. The IVOCs EFs for the China V vehicle ranged from 12.1 to 226.3

24   mg kg-fuel^{-1}, with a median value of 83.7 mg kg-fuel^{-1}, which is higher than that from

25   US vehicles. Besides, large discrepancy in volatility distribution and chemical

26   composition of IVOCs from Chinese gasoline vehicle exhaust is discovered, with

27   larger contributions of B_{14}-B_{16} compounds and higher percentage of n-alkanes. Further

28   we investigated the possible reasons that influence the IVOCs EFs and volatility

29   distribution and found that fuel type, starting mode, operating cycles and acceleration

30   rates could have an impact on the IVOCs EF. When using E10 (ethanol volume ratio

31   of 10%, v/v) as fuel, the IVOCs EF of the tested vehicle was lower than that using

32   commercial China standard V fuel. Cold-start operation has higher IVOCs EF than

33   hot-start operation. Chinese Light vehicles Test Cycle (CLTC) produced 70% higher

34   IVOCs than those from the World-wide harmonized Light-duty Test Cycle (WLTC).

35   We found that vehicle emitted more IVOCs at lower acceleration rates, which leads to

36   high EFs under CLTC. The only factor that may influence the volatility distribution

37   and compound composition is the engine-aftertreatment system, which has compound

38   and volatility selectivity in exhaust purification. These distinct characteristics in EFs

39   and volatility may result in higher SOA formation potential in China. Using published

40   yield data and surrogate equivalent method, we estimated SOA formation under

41   different OA loading and NO$_x$ conditions. Results showed that under low and high

42   NO$_x$ conditions at different OA loadings, IVOCs contributes more than 80% of the

43   predicted SOA. Furthermore, we built up a parameterization method to simply

44   estimate the vehicular SOA based on our bottom-up measurement of VOCs and

45   IVOCs, which would provide another dimension of information when considering the

46   vehicular contribution to the ambient OA. Our results indicate that vehicular IVOCs

47   contribute significantly to SOA, implying that the importance of reducing IVOCs

48   when making air pollution controlling policies in urban area of China.

49

1 Introduction

Atmospheric fine particulate matter has great impacts on human health, climate, and global environmental issues (Tang et al., 2018;Guo et al., 2014b;Hallquist et al., 2009;Kanakidou et al., 2005). Organic aerosols are a major component of fine particulate matter. Secondary organic aerosol (SOA), formed from multiple generations of oxidation of thousands of organic gases and vapors, contribute 30% or more of organic aerosols in different areas of the world (Zhang et al., 2007). Due to its complexity in sources and photochemical processes, SOA formation remains uncertain (Tang et al., 2019;Guo et al., 2014a).

A large discrepancy remains between modeled and measured SOA. One possible reason is missing SOA precursors. Apart from traditional SOA precursors, i.e. volatile organic compounds (VOCs), Robinson et al. (2007) proposed intermediate volatility organic compounds (IVOCs) as important contributors to SOA formation. IVOCs are less volatile than VOCs with effective saturation concentrations in the range of 10^3 to 10^6 $\mu g/m^3$(Donahue et al., 2006), roughly corresponds to the volatility range of C_{12}-C_{22} n-alkanes. IVOCs exist mainly in the gas phase under typical atmospheric conditions. Previous studies demonstrate that IVOCs may be important SOA precursors both in ambient air and in typical source emissions i.e. gasoline vehicles, diesel vehicles and ship emissions (Huang et al., 2018;Zhao et al., 2016, 2015;Zhao et al., 2014).

China is in a high-growth stage with rapidly increasing number of on-road vehicles (~26 fold in 25 years). This growth has created a substantial burden on air quality and human health (Hallquist et al., 2016;Hu et al., 2015). During the past few years, many researchers have studied the gases and particulate matter emissions from Chinese vehicles (Cao et al., 2016;Huang et al., 2015). However, none of these studies have reported data on IVOCs emissions from Chinese gasoline vehicles. Although Zhao et al. (2016) characterized IVOC emission in gasoline vehicles in the United States, the results may not be applicable to China given differences in vehicle technologies, operating conditions, and fuel quality. Therefore, characterizing the IVOC emissions from Chinese vehicle is of vital importance to understand the

80 contribution of IVOCs contribution to SOA formation in China(Zhao et al.,

81 2018;Zhao et al., 2016, 2015;Zhao et al., 2014).

82   In this study, IVOCs emissions were measured from a China V gasoline vehicle

83 equipped with a direct inject (GDI) engine during chassis dynamometer testing. The

84 test matrix considered the influence of fuel type and operating conditions on the total

85 IVOC emission factors, including a newly designed cycle designed to simulate

86 Chinese driving conditions. All of the measurements were performed with the same

87 gasoline vehicle in order to consistently evaluate the effects of these different factors

88 on IVOC emissions. The emission factors (EFs), volatility and chemical speciation of

89 IVOC emissions from different conditions were investigated, and the SOA formation

90 potential were estimated.

91

92 2 Materials and Methods

93 2.1 Testing Vehicle, Fuels and Test Cycles

94   In this study, all measurements were performed on a vehicle chassis

95 dynamometer (Peng et al., 2017) using an in-use light-duty gasoline direct inject (GDI)

96 engine vehicle meeting the China V standard (similar to Euro 5). Tests were

97 conducted with two fuels: commercial China Standard V gasoline and E10 fuel (10%

98 ethanol by volume). The test cycles included the World-wide harmonized Light duty

99 Test Cycle (WLTC), and the Chinese Light vehicles Test Cycle (CLTC). Furthermore,

100 typical different acceleration rates were also tested. Detailed description and speed

101 profiles of WLTC and CLTC are in Figure S1 in the supplementary information. The

102 CLTC was specifically designed to simulate the driving patterns in Chinese cities

103 while WLTC referred to the Euro VI standard and adopted as China VI testing

104 protocol. Prior to tests, vehicles were preconditioned with an overnight soak, without

105 evaporative canister purge. Different acceleration rates were selected based on their

106 frequency in both CLTC and WLTC, i.e. 1.2, 3.6 6.0 km/h/s, written as ACR1.2,

107 ACR3.6 and ACR6.0), to investigate the effects of acceleration rates on IVOC

108 emissions. All three acceleration "cycles" last for 600 s with a maximum velocity of

109 70 km/h. The acceleration driving cycles were set according to the criteria of identical

110   cycle period and maximum velocity, and hence the mean velocity for each

111   acceleration cycle is the same (Figure S2). We also measured IVOC emission factors

112   (EFs) when the test vehicle was idling.

113

114   **2.2 Sampling and Chemical Analysis**

115   Tailpipe emissions were introduced to a constant volume sampler (CVS) that

116   diluted the exhaust by a factor of 20 to 40. For WLTC and CLTC tests, IVOCs

117   emissions were collected by sampling the diluted exhaust through a quartz filter

118   followed by two tandem Tenax TA filled glass tubes (Gerstel, 6 mm OD, 4.5 mm ID

119   glass tube filled with ~180 mg Tenax TA). Sampling tubes and transfer lines from the

120   CVS were kept at a constant temperature (27 ± 2 °C). The flow rate for quartz filter

121   was 10.0 L/min, and the flow rate for Tenax tube was set as 0.5 L/min. Dynamic

122   blanks were also collected when the CVS was operated with only dilution air (no

123   exhaust) to estimate the contribution of background organic vapors. Prior to sampling,

124   the quartz filters were preheated to 550 °C in air for 6 h in clean aluminum foil using

125   a muffle furnace to remove contaminations. Tenax tubes were preconditioned by using

126   Tube Conditioner (BCT700, BCT Technology LTD), at 300 °C for 3 h in pure

127   nitrogen with a constant flow rate of 100 mL/min. All samples were sealed after

128   sampling and stored in freezer at -20°C.

129   Quartz filters and Tenax tubes were analyzed using gas chromatography/mass

130   spectrometer (Agilent 6890GC/5975MS) equipped with a capillary column (Agilent

131   HP-5MS, 30 m$\times$0.25 mm) coupled to a thermal desorption system (Gerstel, Baltimore,

132   MD). The detailed method was described in the literature by Zhao et al.(2014). Prior

133   to analysis, 5 μl of the internal standards (*d*10-acenaphthene, *d*12-chrysene,

134   *d*4-1,4-dichlorobenzene, *d*8-naphthalene, *d*12-perylene, *d*10-phenanthrene and 7

135   deuterated *n*-alkanes) were injected into each adsorbent tube to track the IVOCs

136   recovery.

137   For each test, particulate matter samples were also collected using independent

138   Teflon and quartz filters. The Teflon filters were weighted using a microbalance

139   (Toledo AX105DR, USA) after equilibration for 24 h in an environmental controlled

140   room (temperature $20 \pm 1^{\circ}C$, relative humidity $40 \pm 3\%$) (Guo et al., 2010). A punch

141   (1.45 cm^2) from each quartz filter was analyzed for organic carbon (OC) and

142   elemental carbon (EC) via thermal-optical method using Sunset Laboratory-based

143   instrument (NIOSH protocol, TOT) (Guo et al., 2012). VOCs were sampled in

144   SUUMA canisters and analyzed using GC-MS with a flame ionization detector. Total

145   hydrocarbon (THC), nitrogen oxide, CO and CO_2 emissions under operation scenarios

146   were measured using a Horiba OBS 2200 portable emission system.

147

148   **2.3 Quantification of IVOCs**

149   Twenty IVOCs compounds were quantified using authentic standards (Table S1).

150   However, the majority of the IVOCs mass appears as a broad hump of co-eluting

151   hydrocarbons and oxygenated organics. These compounds could not be resolved at

152   the molecular level and were therefore classified as an unresolved complex mixture

153   (UCM), which were grouped based on their volatilities.

154   The total mass of IVOCs was determined following the method of Zhao et al.

155   (2014) (SI) . In short, the TIC of each sample was divided in to 11 retention time bins

156   corresponding to C_{12}-C_{22} n-alkanes. The total mass in each bin was estimated using

157   the instrument response to the n-alkane in that bin. UCM was determined as the

158   difference between total IVOCs and speciated IVOCs in each bin. UCM was then

159   further classified into unspeciated branched alkanes (b-alkanes) and unspeciated

160   cyclic compounds following the approach of Zhao et al. (2016) (SI).

161   Fuel-based IVOC emission factor (EF, mg/kg-fuel) were calculated using the

162   carbon-mass-balance method as following

163    $$\text{EF}_{\text{IVOCs}} = \frac{[\Delta IVOC]}{[\Delta CO_2]} f_c$$

164   where $[\Delta IVOC]$ represents the background-corrected mass concentration of

165   IVOCs, $[\Delta CO_2]$ is the background-corrected CO_2 concentration in the CVS expressed

166   in units of carbon mass and f_c is the measured mass fraction of carbon in the gasoline

167   (0.82).

168

169 **3 Results and Discussion**

170 **3.1 Influence of Fuel, Starting Mode, and Operating Cycles on IVOC Emission**

171 **Factors**

172   Figure 1 depicts IVOC EFs of the tested China V gasoline vehicle and compares

173 them with previous studies. The IVOC EFs ranged from 12.1 to 226.3 mg kg-fuel^{-1},

174 with a median value of 83.7 mg kg-fuel^{-1}. The median IVOC value was ~3 times

175 higher than that of the US LEV-2 gasoline vehicles (21.9 mg kg-fuel^{-1}), and one order

176 of magnitude lower than diesel-fueled non-road construction machinery and a

177 diesel-fueled large cargo vessel (971.1 and 800 mg kg-fuel^{-1}, respectively) (Qi et al.,

178 2019;Huang et al., 2018).

179   Figure 1 summarizes the influences of fuel type, starting mode, operating cycles

180 and acceleration rates on the total IVOC EFs. Among all of the factors, acceleration

181 rate has the largest influence on the IVOC EFs. As the acceleration rate increases, the

182 IVOC EF decreases, with the median IVOC EF of ACR6.0 being one order of

183 magnitude lower than that at idling. Qi et al. (2019) and Zhao et al. (2016) report

184 similar results for non-road construction machinery and on-road diesel vehicles,

185 where idling conditions emitted significantly higher IVOCs than those under

186 higher-speed cycles. They proposed that the higher IVOC EFs at idling were the result

187 of less efficient fuel combustion. An additional factor in these tests may be the

188 efficiency of the catalytic converter varying with operating conditions (i.e. lower

189 efficiency at idle operations).

190   When using commercial China Standard V gasoline, the median IVOC EF was

191 1.4 times greater than that using Ethanol gasoline, i.e. E10 (10% ethanol, v/v), with

192 median values of 91.5, and 67.6 mg kg-fuel^{-1}, respectively. The median THC EFs for

193 gasoline and E10 were 485 and 589 mg kg-fuel^{-1}, respectively, showing no significant

194 difference.

195   As expected, The IVOC EFs for cold-start tests was higher (83.7 mg kg-fuel^{-1})

196 than those for hot-start tests (58.7 mg kg-fuel^{-1}). This reflects the reduced efficiency

197 of the catalytic converter during cold-start operation. The cold-start to hot-start IVOC

198 emission ratio is about 1.4, which is similar to the previous study (Zhao et al., 2016).

199   The median THC EFs for cold-start and hot-start tests are 556.2 and 507.8

200   mg kg-fuel^{-1}, respectively. Previous studies also show that cold starts have higher

201   THC EFs than hot start operation, but cold-to-hot ratios can span a wide range due to

202   differences in operating conditions and model years(Jaworski et al., 2018;Drozd et al.,

203   2016). The ratio is generally larger for more modern, heavily controlled

204   vehicles(Saliba et al., 2017;May et al., 2014).

205   The median IVOC EF for CLTC was about 1.7 times of that for WLTC (103.5

206   versus 60.9 mg kg-fuel^{-1}). Similar results were also found for THC emission, with

207   median THC EFs for CLTC and WLTC cycle as 617.3 and 420.3 mg kg-fuel^{-1},

208   respectively. Previous studies also show test cycles influence THC EFs. For example,

209   Suarez-Bertoa et al. (2015) and Marotta et al. (2015) found NEDC cycle has higher

210   THC EFs than WLTP or WLTC cycle. One possible explanation for the differences

211   between the CLTC and WLTC IVOC EFs is the differences in acceleration rates. A

212   histogram of acceleration rates of the two cycles (Figure S3) shows that CLTC has

213   frequent low acceleration process compared to WLTC. 76.9% of the CLTC has

214   acceleration rates ranging from -1.5 to 1.5 km/h/s versus 69.6% for the WLTC. The

215   CLTC has no acceleration rate higher than 4 km/h/s, suggesting that the gasoline

216   vehicles frequently drive in congested conditions in China.

217   The results from the acceleration rate cycles suggest that the frequent low

218   acceleration rate in CLTC is responsible for the differences of the IVOC EF between

219   CLTC and WLTC. The effect of acceleration on IVOC EFs is probably especially

220   important in urban areas in China, which frequently have substantial traffic

221   congestion. These results underscore the importance of developing cycles that

222   simulate real-world Chinese driving condition e.g. CLTC, instead of using WLTC or

223   other cycles to get relevant emissions data.

224

225   **3.2 Chemical Speciation of Chinese Vehicle IVOCs and the Relationships**

226   **between Total IVOCs, POA and THC**

227   Figure 2 and S4 compare the chemical composition of IVOC emissions from the

228   tested China V vehicle under different operating conditions. In general, IVOC

229 chemical composition was similar across all the tests. Unspeciated IVOCs (UCM)

230 dominates the total IVOCs mass ($85.6 \pm 4.9\%$), including $65.2 \pm 5.2\%$ for unspeciated

231 cyclic compounds and $20.4 \pm 0.7\%$ for unspeciated b-alkanes. n-alkanes and speciated

232 aromatics contribute $10.9 \pm 4.7\%$ and $3.5 \pm 1.7\%$ of the total IVOC mass, respectively.

233 These results are similar to previous studies. For example, Zhao et al. (2016) found

234 the consistent composition of IVOC emissions across a wide set of vehicles.

235   Since the majority of the IVOC mass appears as UCM, the average mass spectra

236 provide additional insight into its composition. A similar distribution of mass

237 fragments was observed across all tests. Figure 2(b) shows the average IVOC mass

238 spectrum collected during an E10 CLTC test. Mass fragments associated with

239 aliphatic hydrocarbons (m/z 43, 57, 71, 85) are the most abundant followed by those

240 associated with aromatics (m/z 91, 105 and 119 for alkylbenzenes (Pretsch et al.,

241 2013), and m/z 115, 165, 189 for poly aromatic species) (Dall'Osto et al.,

242 2009;Spencer et al., 2006).

243   Figures 2(c) and (d) exhibit the contribution of selected mass fragments in low

244 and high volatility ranges, i.e. B_{12}-B_{16} and B_{17}-B_{22}. Aliphatic fragments are higher than

245 aromatics fragments in both B_{12}-B_{16} and B_{17}-B_{22} bins. Compared to the higher

246 volatility (B_{12}-B_{16}) bins, the ratio of selected aromatic to aliphatic fragments is lower

247 in the lower volatility (B_{17}-B_{22}) bins (0.8 versus 1.7) which suggests different

248 weighting of compounds in different volatility range. Therefore, unspeciated IVOC

249 UCM in B_{12}-B_{16} are predominantly aromatics while B_{17}-B_{22} are more abundant in

250 cyclic alkanes.

251   Figure 3 and S5 shows the volatility distribution of IVOC emissions in the 11

252 retention-time bins (B_{12}-B_{22}). IVOC emissions are more heavily weighted towards the

253 more volatile end of the distribution, with more than 50% of the emissions in B_{12}-B_{14}

254 bins. After B_{14}, the IVOC emission decreases significantly.

255   Although the IVOC EFs varied by an order of magnitude across the set of tests

256 (Figure 1), the volatility distributions of the emissions were largely the same. When

257 the vehicle is fueled by gasoline, the median IVOC fractions in the B_{12}-B_{14} bins are

258 slightly higher than when fueled by E10. Cold-start having a higher median

259 percentage of IVOC in B_{12}-B_{14} bins compared to hot-start. No distinct differences in

260 volatility differences between the CLTC and WLTC. Compared with idling condition,

261 acceleration cycles have higher median percentage of IVOC in lower volatility bins

262 (B_{17}-B_{22}), similar to previous studies (Qi et al., 2019;Cross et al., 2015).The modest

263 variations of volatility distributions of the IVOCs emissions may be due to differences

264 in combustion efficiency and/or catalytic converter efficiency as a function of

265 volatility.

266 Previous studies have used different scaling approaches to estimate IVOC

267 emissions using other primary emission data, e.g. POA, NMHC (Murphy et al.,

268 2017;Woody et al., 2016;Koo et al., 2014). However, these ratios depend on fuel,

269 engine technology and operating conditions (Lu et al., 2018).Therefore, it is important

270 to quantify the relationships between IVOCs and other pollutants using data collected

271 from Chinese vehicles. Our results show that the IVOC-to-THC ratio does depend on

272 fuel composition. The average IVOC-to-THC ratios for gasoline-fueled and

273 E10-fueled gasoline vehicle are 0.07 $\pm$ 0.01(R^2 = 0.87) and 0.11 $\pm$ 0.02 (R^2 = 0.78),

274 respectively (Figure S6). The IVOC-to-THC ratios in this study are higher than US

275 vehicles (IVOC-to-NMHC of 0.04) (Zhao et al., 2016) but much lower than diesel

276 fueled vehicles (IVOC-to-THC of 0.67) (Huang et al., 2018). The IVOC-to-POA ratio

277 was 5.12 $\pm$ 1.30 across all tests, but with only modest correlation (R^2 of 0.66 for

278 gasoline-fueled vehicle and 0.43 for E10-fueled vehicle). This ratio is similar to US

279 data for gasoline vehicles. The correlation of IVOC to THC or POA in our dataset is

280 lower than that of the on-road gasoline and diesel vehicles measured in US. This may

281 be caused to the US data are from a large fleet of vehicles while our data is from a

282 single vehicle operated over a range of conditions

283

284 **3.3 High Emission Factors and Distinct Volatility Distributions of IVOCs from**

285 **Chinese Gasoline Vehicles**

286 Figure 4 presents PM, NO$_x$, THC and IVOC EFs of the tested gasoline vehicle

287 (China V) and compares them to US vehicles tested by Zhao et al. (Zhao et al.,

288 2016;May et al., 2014) For this comparison, we combined all of the CLTC and WLTC

289   data together. The US vehicles are grouped by model year where pre-LEV refers to

290   vehicles manufactured prior to 1994, LEV-1 represents vehicles manufactured

291   between 1994-2003, and LEV-2 indicates vehicles manufactured between 2004-2012.

292   The emissions of NO_x and THC from tested vehicle are comparable with those

293   from the newer (LEV-2) US vehicles tested by May et al. (Zhao et al., 2016;May et al.,

294   2014). However, PM EF (44.8 mg kg-fuel^{-1}) of the tested vehicle is higher than the

295   LEV-2 vehicles tested (17.0 mg kg-fuel^{-1}). It is comparable to a pre-LEV vehicle

296   (61.0 mg kg-fuel^{-1}). This suggests that stringent emission implemented by Chinese

297   government have been effective at controlling NO_x and THC, but inefficient to PM

298   emissions.

299   The IVOC EFs for the tested China V vehicle is between the US Pre-LEV and

300   LEV-1 vehicle. Therefore, Chinese regulations also appear to be ineffective at

301   controlling IVOC emissions. The IVOC-to-THC ratio measured here (0.07 for

302   gasoline and 0.11 for E10) is higher than US vehicles (0.04), which means that IVOCs

303   contribute a larger fraction of the THC emissions from the China V than from the US

304   vehicles. A detailed comparison of the individual VOC emissions between China V

305   and US LEV-2 vehicles is in SI (Table S8).

306   UCM accounts for large fraction of IVOCs for both China V and US gasoline

307   vehicles. However, the speciated compounds exhibit different characteristics. The

308   China V exhaust has less speciated IVOC aromatic compounds (3.5%) and more

309   alkanes (10.9%) compared to US exhaust (12.9% and 2.5%, respectively). This is also

310   reflected by the IVOC mass spectrum, where Chinese vehicle exhaust has higher *m/z*

311   43, 57, 71, 85 signals. In addition, the specific aromatics mass fragments were not the

312   same for China V and US IVOC emissions. For example, the dominant aromatics

313   fragments in US gasoline exhaust are *m/z* 128, 119, 105, 133 versus *m/z* 135, 91, 181,

314   189 for China V. (Fig. 2c and d).

315   Figure 3 compares the volatility distribution of the IVOC emissions from the

316   China V and US vehicles. There are significant differences of volatility distribution

317   between China V and US vehicles. Both distributions decrease with the increase of

318   the retention time, but the IVOC volatility distribution of US vehicle exhaust exhibits

319   heavier weight of lower volatility bin, i.e. B_{12} bin compared to the China V vehicle. In

320   US exhaust the B_{12} fraction is more than double of the B_{13}. However, the contributions

321   of B_{12}-B_{14} bin volatility bins are comparable for Chinese vehicle exhaust. US vehicle

322   exhaust has a similar IVOC volatility distribution to the unburned gasoline, indicating

323   that the evaporate of IVOCs from fuel is non neglectable.

324   The differences between the IVOC volatility distribution between the Chinese

325   vehicle exhaust and unburned gasoline were further investigated. The higher emission

326   factor and broader distribution of IVOCs in exhaust from China V compared with US

327   vehicles may be due to differences in fuel composition, operating conditions and

328   engines and after-treatment technology. Lu et al. (2018) demonstrated that IVOC

329   emissions depend strongly on fuel composition. In our study, IVOCs contributed ~2.0

330   wt% (2.1 wt% for gasoline, 1.9 wt% for E10) of the total fuel mass, which is ~60%

331   higher than the California fuel (E10, 1.2 wt%)(Gentner et al., 2012). Therefore, the

332   higher IVOC fractions in China V exhaust (e.g. IVOC-to-THC ratio of 0.07 and 0.11

333   versus 0.04 in US exhaust) may lead to higher amounts of IVOCs in China V gasoline.

334   When considering volatility distribution, Zhao et al. (2016) and Lu et al. (2018)

335   reported similar distributions of IVOC between gasoline vehicle exhaust and

336   unburned fuel, which demonstrates the significant influence of unburned fuel on

337   exhaust volatility distribution. However, the volatlity distribution of the China V

338   gasoline vehicle exhaust are different from that of the unburned fuel (Figure 3). The

339   difference might be related to the operating conditions and engine-aftertreatment

340   system.

341   Although operating conditions strongly influence the total IVOC EFs (Figure 1),

342   Figure 3 indicates the volatility distribution of the IVOCs emissions were largely

343   consistent across the set of test conditions. Therefore, operating conditions cannot

344   explain the difference in the IVOC volatility distribution between the China V vehicle,

345   unburned gasoline, and the US vehicles.

346   The engine-aftertreatment system also influences IVOC emissions (Drozd et al.,

347   2019;Alam et al., 2019;Zhao et al., 2018;Saliba et al., 2017). In order to investigate

348   the efficiency of after-treatment system, we normalized the IVOC distributions of the

349 fuel and exhaust to the sum of C_8-C_{10} *n*-alkanes. It is believed that the C_8-C_{10}

350 *n*-alkanes can serve as the indicators for VOCs in fuel (Lu et al. 2018). For both US

351 and the China V vehicles, IVOCs are enriched in the exhaust relative to the fuel.

352 However, the enrichment factor is much smaller in Chinese exhaust with a median

353 value of 4.0 than that   for US vehicles (median value = 8.5) (Lu et al., 2018). The

354 enrichment factor also varies with different compounds, with the enrichment factors

355 of *n*-alkanes (9.3)＞*b*-alkanes (6.6)＞unspeciated cyclic ompounds (3.1)＞aromatics

356 (0.4). These results are consistent with previous studies stating that the aftertreatment

357 devices have different removal efficiency towards different compounds (Ma et al.,

358 2019;Hasan et al., 2018;Hasan et al., 2016;Alam and Harrison, 2016). Our results

359 suggest that the Chinese three-way catalytic converter has compound dependent

360 efficiency (better removal of aromatics compared to alkanes) which might explain the

361 difference in compound composition between Chinese and US vehicle exhaust.

362 Furthermore, Fig. S9 shows that the catalytic converter has different removal capacity

363 towards different volatility bins, in which B_{14-16} works much worse compared to other

364 volatility bins i.e. B_{12}. Consequently, the SOA formation would be relatively high. In

365 sum, the compound dependent capacity and lower B_{14}-B_{16} removal efficiency of

366 Chinses TWC is responsible for the volatility distribution differences between China

367 V and US vehicles shown in Figure 3.

368   After considering all the factors above, we can draw the conclusion that fuel type,

369 starting mode and operating conditions can all affect the IVOCs EFs. The only factor

370 that impacts the volatility distribution is engine-aftertreament system.

3.4 Estimation of SOA Production from Chinses Vehicle Emission

372   With the measured IVOC and VOC emissions, we estimated the SOA formation

373 potential by using the yield method as following (Yuan et al., 2013):

374       $$\Delta SOA/\Delta CO = \sum ER_{[HC]_i} \times \left(1 - e^{-(k_{OH,i}-k_{CO})\times[OH]\times\Delta t} \right) \times Y_i$$

375   In which, $ER_{[HC]_i}$ is the emission ratio of SOA precursor i (mg kg-fuel^{-1}); $k_{OH,i}$

376 is the OH reaction rate constant of precursor i at 298K (cm^3 molecules^{-1} s^{-1}); k_{CO} is

377 the OH reaction constant of CO at 298 K (2.4×10^{-13} cm^3 molecules^{-1} s^{-1}); [OH] is the

378   OH mixing ratio, which is assumed to be 1.5×10^6 molecules cm^3 (Lu et al., 2019); Δt

379   is photochemical age (h); and Y_i is the SOA yield determined from chamber studies.

380   Previous studies have shown that the SOA yield of individual hydrocarbon can be

381   influenced by NO_x level, due to the competition reactions among RO_2 radicals, NO

382   and HO_2 radicals. Usually SOA yields under low NO_x condition are independent on

383   the OA loading. However, under high NO_x condition, SOA yields highly depend on

384   OA mass concentration, which can be described using two-product or multi-products

385   model (Presto et al., 2010;Chan et al., 2009;Ng et al., 2007). In this study, we

386   estimated SOA formation under low and high NO_x conditions with OA concentration

387   of 10, 20, 80 μg·m^{-3} to represent the influence of NO_x level and OA loading on SOA

388   formation.

389   In this estimation, we include speciated C_6-C_9 single ring aromatics (SRAs) as

390   typical VOCs for SOA precursors, and the corresponding k_{OH} and SOA yields are

391   extrapolated according to two-product relationship from chamber studies (see SI) (Ng

392   et al., 2007). The SOA yields under low and high NO_x condition, and the OH reaction

393   rates of speciated IVOCs and SRAs are from the previous studies (see SI) (Presto et

394   al., 2010;Lim and Ziemann, 2009;Chan et al., 2009). In brief, surrogate species were

395   used to represent the unspeciated b-alkanes and cyclic compounds in each of the

396   volatility bins.

397   Figure 5 shows the POA emission and estimated SOA production under different

398   operating conditions and NO_x level after 48 h of photo-oxidation. The estimated

399   SOA/POA ratio is between 4.0 to 5.0 under low NO_x condition, and the SOA-to-POA

400   ratios ranged from 1.8-2.2 to 3.8-4.4 when the OA loading increased from 10 μg·m^{-3}

401   to 80 μg·m^{-3} under high NO_x condition. The OA enhancement under low NO_x

402   condition is similar to that under high NO_x condition with the OA loading of 80

403   μg·m^{-3}. Considering the high POA concentration and SOA formation capacity of

404   Chinese gasoline vehicles, the SOA/POA ratios at 80 μg·m^{-3} are considered as a lower

405   estimation. Compared with OA enhancement from US studies (~3.6) (Zhao et al.,

406   2016), our results showed higher SOA formation potential both under low and high

407   NO_x conditions for Chinese gasoline vehicles.

408   Scenario-based analysis showed similar tendency of SOA formation potential at

409   different OA loading under low and high NO$_x$ condition. Comparable SOA formation

410   was estimated using gasoline and E10 as fuel. However, the OA enhancement factor

411   for E10 is higher than that of gasoline, suggesting that although the ongoing policy of

412   ethanol gasoline will not exacerbate the POA and SOA pollution in China, the OA

413   enhancement capacity of E10 could not be neglected. More research should be done

414   to evaluate the effectiveness of using E10 as surrogate to reduce the air pollution in

415   China. Cold-start operation has higher SOA potential with higher OA enhancement

416   factor than hot-start, due to the higher precursors EFs caused by the reduced catalytic

417   converter effectiveness below its light off temperature(Drozd et al., 2019). The IVOC

418   EFs, the estimated SOA production and SOA/POA of CLTC are all higher than those

419   of WLTC, which further demonstrates the higher SOA formation potential of Chinese

420   gasoline vehicles under typical driving conditions in China.

421   Figure S10 presents the contribution of different classes of precursors on the

422   SOA production after 48 h of photo-oxidation under different OA loading and NO$_x$

423   condition. The relative contributions of different chemical classes were similar across

424   the different conditions, with the largest contribution from unspeciated cyclic IVOCs.

425   This is different from the US gasoline vehicle SOA (Zhao et al., 2016) in which single

426   ring aromatics contributes the most.

427

428   **3.5 Establishing the Estimation Method of SOA formation from Chinese**

429   **Gasoline Vehicles**

430   In this section, we tried to establish parameterization methods to provide simple

431   estimations of gasoline vehicle SOA based on our measurements of VOCs and

432   IVOCs.

433   Figure S11 shows the average predicted SOA-to-POA ratio as the function of

434   photo-oxidation time under different OA loading and NO$_x$ conditions. In general,

435   SOA exceeds POA after first a few hours of oxidation, and then keeps constant after

436   ~24 h. The SOA/POA ratio is influenced by OA concentration, NO$_x$ level and the

437   photochemical age (OH exposure). At a certain OA loading and OH exposure,

438   SOA/POA ratio can be estimated, and then be used to quantify the contributions of

439   gasoline vehicle SOA to the ambient OA. Therefore, we parameterized the SOA/POA

440   variation under different OA and NO_x condition using three-parameter-based

441   logarithm equation, i.e. y=a-b×ln(t+c), in which t represents the equivalent

442   photochemical age (assume that the OH concentration is 1.5×10^6 molecules cm^3) and

443   a, b, c can be described using three-parameter logarithm equation y=m-n×ln([OA

444   concentration]+p). Table 1 shows the parameterization results of compounds-based

445   SOA/POA variation under the different OA and NO_x condition.

446

447

448   Table 1 Coefficient of parameterization between SOA/POA and photochemical age

SOA/POA	Low NO_x condition	High NO_x condition		
		m	n	p
a	-0.62	0.46	0.22	9.8
b	1.34	0.27	0.33	2.58
c	0.58	0.13	-0.09	3.35
Unspeciated cyclic compounds				
a	-0.15	0.26	0.09	21.76
b	0.72	0.086	0.18	0.46
c	0.11	-0.278	-0.083	24.42
Unspeciated b-alkanes				
a	-0.11	0.47	0.111	87.54
b	0.17	0.15	0.070	12.36
c	0.84	-0.17	-0.21	41.97
aromatics				
a	-0.03	-0.023	-0.0098	40.52
b	0.03	0.012	0.007	17.27
c	-1.00	-1.02	-0.021	-10.00
n-alkanes				
a	-0.05	0.0067	0.013	-2.38
b	0.11	0.019	0.030	-0.52

c	0.48	0.15	-0.058	29.18
Single ring aromatics				
a	-0.51	0.28	0.17	5.47
b	0.35	0.03	0.059	-2.29
c	3.92	2.80	-1.29	10.84

449   The above photochemical-based parameterization method provides a conservative

450   way to quantify the evolution of SOA from Chinese gasoline vehicle VOCs and

451   IVOCs oxidation. However, there are still some uncertainties which may lead to

452   discrepancies between predicted and measured SOA. In general, positive or negative

453   artifacts of quartz filters, n-alkane equivalent method in estimating the IVOCs

454   concentration, uncertainty in SOA yield, surrogate method to substitute SOA yield

455   and k_{OH} for UCM and lack of semi-volatile organic compounds will exert influence on

456   the SOA prediction.

457

458   **4 Atmospheric Implications**

459   We measured the VOCs, IVOCs and POA emitted from a China V light duty

460   gasoline vehicle across a wide range of operating conditions. Compared with US

461   LEV-2 gasoline vehicle, China V vehicle emits three times higher IVOCs. Besides,

462   the IVOC emissions from the China V vehicle have a much broader volatility

463   distribution than that from US vehicles. These characteristics imply that IVOCs could

464   act more important SOA precursors in China than those in the US. For Chinese

465   gasoline vehicles, although the magnitude of the emission of IVOCs and VOCs can

466   vary, their relative contribution to SOA production is similar across the set of

467   operating conditions examined here due to the similar volatility distributions. As a

468   result, the key to control SOA formation of gasoline vehicles is to reduce the total

469   IVOC EFs by upgrading of emissions controls. In addition, reducing congestion and

470   other low speed operating modes would also be effective at reducing emissions

471   (Figure 1 and 5).

472   Based on our results, we roughly estimate the vehicle IVOC emissions in China.

473   Till the end of 2018, the HC emission of gasoline vehicles in China was 0.23 Mt,

474   accounting for more than 70% of the total vehicle emissions. Using an IVOC/THC

475   ratio of 0.09 that is obtained in our work, we estimate that the vehicle IVOC

476   emissions in China are 0.03 Mt (30 Gg), in which 20 Gg is attributed to gasoline

477   vehicles. One should note that this estimation is a conservative value, since we

478   consider all vehicles as gasoline vehicles, and all of them meet the China V standard.

479   Considering the IVOC/NMHC ratio of diesel vehicles could be much higher than that

480   of the gasoline vehicles(Zhao et al., 2016, 2015). This may also lead to an

481   underestimation.

482   Our results show that using a Chinese real-world test protocol CLTC will result

483   in substantially higher IVOC emissions compared with WLTC which might have

484   close relationship with frequent idling and low acceleration condition. Therefore,

485   when driving at typical Chinese condition where traffic congestion frequently occur,

486   the IVOCs emission from Chinese gasoline vehicles would be much higher than the

487   current limited emission inventory. Our results indicate simply controlling the THC,

488   NO_x and primary PM emissions may be insufficient in the aspect of controlling

489   particle pollution. Reducing IVOC emissions should also be taken into consideration

490   due to their high contribution to SOA formation, which is more important than

491   primary organic aerosol. Suggested controlling ways include upgrading the fuel

492   quality and engine-after treatment system, and reducing the traffic congestion.

493

494   **Acknowledgement**

495   This research is supported by the National Natural Science Foundation of China (No.

496   41977179,51636003,21677002,91844301), the Open Research Fund of State Key

497   Laboratory of Multi-phase Complex Systems (MPCS-2019-D-09). ALR and QY

498   received financial support from the Center for Air, Climate, and Energy Solutions

499   (CACES), which was funded by Assistance Agreement No. RD83587301 awarded by

500   the U.S. Environmental Protection Agency. It has not been formally reviewed by EPA.

501   The views expressed in this document are solely those of authors and do not

502   necessarily reflect those of the Agency. EPA does not endorse any products or

503   commercial services mentioned in this publication.

504

References

506 Alam, M. S., and Harrison, R. M.: Recent advances in the application of 2-dimensional gas
507 chromatography with soft and hard ionisation time-of-flight mass spectrometry in environmental
508 analysis, Chemical Science, 7, 3968-3977, 10.1039/c6sc00465b, 2016.

509 Alam, M. S., Zeraati-Rezaei, S., Xu, H., and Harrison, R. M.: Characterization of Gas and Particulate
510 Phase Organic Emissions (C9–C37) from a Diesel Engine and the Effect of Abatement Devices,
511 Environmental science & technology, 53, 11345-11352, 2019.

512 Cao, X., Yao, Z., Shen, X., Ye, Y., and Jiang, X.: On-road emission characteristics of VOCs from
513 light-duty gasoline vehicles in Beijing, China, Atmospheric Environment, 124, 146-155,
514 https://doi.org/10.1016/j.atmosenv.2015.06.019, 2016.

515 Chan, A. W. H., Kautzman, K. E., Chhabra, P. S., Surratt, J. D., Chan, M. N., Crounse, J. D., Kuerten,
516 A., Wennberg, P. O., Flagan, R. C., and Seinfeld, J. H.: Secondary organic aerosol formation from
517 photooxidation of naphthalene and alkylnaphthalenes: implications for oxidation of intermediate
518 volatility organic compounds (IVOCs), Atmospheric Chemistry and Physics, 9, 3049-3060,
519 10.5194/acp-9-3049-2009, 2009.

520 Cross, E. S., Sappok, A. G., Wong, V. W., and Kroll, J. H.: Load-Dependent Emission Factors and
521 Chemical Characteristics of IVOCs from a Medium-Duty Diesel Engine, Environmental Science &
522 Technology, 49, 13483-13491, 10.1021/acs.est.5b03954, 2015.

523 Dall'Osto, M., Harrison, R., Coe, H., and Williams, P.: Real-time secondary aerosol formation during a
524 fog event in London, Atmospheric Chemistry and Physics, 9, 2459-2469, 2009.

525 Donahue, N. M., Robinson, A. L., Stanier, C. O., and Pandis, S. N.: Coupled partitioning, dilution, and
526 chemical aging of semivolatile organics, Environmental Science & Technology, 40, 2635-2643,
527 10.1021/es052297c, 2006.

528 Drozd, G. T., Zhao, Y., Saliba, G., Frodin, B., Maddox, C., Weber, R. J., Chang, M. C. O., Maldonado,
529 H., Sardar, S., Robinson, A. L., and Goldstein, A. H.: Time Resolved Measurements of Speciated
530 Tailpipe Emissions from Motor Vehicles: Trends with Emission Control Technology, Cold Start Effects,
531 and Speciation, Environmental Science & Technology, 50, 13592-13599, 10.1021/acs.est.6b04513,
532 2016.

533 Drozd, G. T., Zhao, Y., Saliba, G., Frodin, B., Maddox, C., Chang, M. C. O., Maldonado, H., Sardar, S.,
534 Weber, R. J., Robinson, A. L., and Goldstein, A. H.: Detailed speciation of intermediate volatility and
535 semivolatile organic compound emissions from gasoline vehicles: effects of cold starts and
536 implications for secondary organic aerosol formation, Environmental Science & Technology, 53,
537 1706-1714, 10.1021/acs.est.8b05600, 2019.

538 Gentner, D. R., Isaacman, G., Worton, D. R., Chan, A. W. H., Dallmann, T. R., Davis, L., Liu, S., Day,
539 D. A., Russell, L. M., Wilson, K. R., Weber, R., Guha, A., Harley, R. A., and Goldstein, A. H.:
540 Elucidating secondary organic aerosol from diesel and gasoline vehicles through detailed
541 characterization of organic carbon emissions, Proceedings of the National Academy of Sciences of the
542 United States of America, 109, 18318-18323, 2012.

543 Guo, S., Hu, M., Wang, Z. B., Slanina, J., and Zhao, Y. L.: Size-resolved aerosol water-soluble ionic
544 compositions in the summer of Beijing: implication of regional secondary formation, Atmospheric
545 Chemistry and Physics, 10, 947-959, 2010.

546 Guo, S., Hu, M., Guo, Q., Zhang, X., Schauer, J. J., and Zhang, R.: Quantitative evaluation of emission
547 controls on primary and secondary organic aerosol sources during Beijing 2008 Olympics,

548   Atmospheric Chemistry and Physics, 13, 8303-8314, 2012.

549   Guo, S., Hu, M., Shang, D. J., Guo, Q. F., and Hu, W. W.: Research on Secondary Organic Aerosols

550   Basing on Field Measurement, Acta Chimica Sinica, 72, 145-157, 10.6023/a13111169, 2014a.

551   Guo, S., Hu, M., Zamora, M. L., Peng, J., Shang, D., Zheng, J., Du, Z., Wu, Z., Shao, M., Zeng, L.,

552   Molina, M. J., and Zhang, R.: Elucidating severe urban haze formation in China, Proceedings of the

553   National Academy of Sciences of the United States of America, 111, 17373-17378,

554   10.1073/pnas.1419604111, 2014b.

555   Hallquist, M., Wenger, J. C., Baltensperger, U., Rudich, Y., Simpson, D., Claeys, M., Dommen, J.,

556   Donahue, N. M., George, C., Goldstein, A. H., Hamilton, J. F., Herrmann, H., Hoffmann, T., Iinuma, Y.,

557   Jang, M., Jenkin, M. E., Jimenez, J. L., Kiendler-Scharr, A., Maenhaut, W., McFiggans, G., Mentel, T.

558   F., Monod, A., Prevot, A. S. H., Seinfeld, J. H., Surratt, J. D., Szmigielski, R., and Wildt, J.: The

559   formation, properties and impact of secondary organic aerosol: current and emerging issues,

560   Atmospheric Chemistry and Physics, 9, 5155-5236, 2009.

561   Hallquist, M., Munthe, J., Hu, M., Wang, T., Chan, C. K., Gao, J., Boman, J., Guo, S., Hallquist, A. M.,

562   and Mellqvist, J.: Photochemical smog in China: scientific challenges and implications for air-quality

563   policies, National Science Review, 3, 401-403, 2016.

564   Hasan, A. O., Abu-jrai, A., Al-Muhtaseb, A. a. H., Tsolakis, A., and Xu, H.: Formaldehyde,

565   acetaldehyde and other aldehyde emissions from HCCI/SI gasoline engine equipped with prototype

566   catalyst, Fuel, 175, 249-256, https://doi.org/10.1016/j.fuel.2016.02.005, 2016.

567   Hasan, A. O., Elghawi, U. M., Al-Muhtaseb, A. a. H., Abu-jrai, A., Al-Rawashdeh, H., and Tsolakis, A.:

568   Influence of composite after-treatment catalyst on particle-bound polycyclic aromatic hydrocarbons–

569   vapor-phase   emitted   from   modern   advanced   GDI   engines,   Fuel,   222,   424-433,

570   https://doi.org/10.1016/j.fuel.2018.02.114, 2018.

571   Hu, M., Guo, S., Peng, J., and Wu, Z.: Insight into characteristics and sources of PM2.5 in the Beijing–

572   Tianjin–Hebei region, China, National Science Review, 2, 257-258, 2015.

573   Huang, C., Wang, H., Li, L., Wang, Q., Lu, Q., De Gouw, J., Zhou, M., Jing, S., Lu, J., and Chen, C.:

574   VOC species and emission inventory from vehicles and their SOA formation potentials estimation in

575   Shanghai, China, Atmospheric Chemistry and Physics, 15, 11081-11096, 2015.

576   Huang, C., Hu, Q., Li, Y., Tian, J., Ma, Y., Zhao, Y., Feng, J., An, J., Qiao, L., Wang, H., Jing, S. a.,

577   Huang, D., Lou, S., Zhou, M., Zhu, S., Tao, S., and Li, L.: Intermediate Volatility Organic Compound

578   Emissions from a Large Cargo Vessel Operated under Real-world Conditions, Environmental Science

579   & Technology, 52, 12934-12942, 10.1021/acs.est.8b04418, 2018.

580   Jaworski, A., Kuszewski, H., Ustrzycki, A., Balawender, K., Lejda, K., and Woś, P.: Analysis of the

581   repeatability of the exhaust pollutants emission research results for cold and hot starts under controlled

582   driving cycle conditions, Environmental Science and Pollution Research, 25, 17862-17877,

583   10.1007/s11356-018-1983-5, 2018.

584   Kanakidou, M., Seinfeld, J., Pandis, S., Barnes, I., Dentener, F., Facchini, M., Dingenen, R. V., Ervens,

585   B., Nenes, A., and Nielsen, C.: Organic aerosol and global climate modelling: a review, Atmospheric

586   Chemistry and Physics, 5, 1053-1123, 2005.

587   Koo, B., Knipping, E., and Yarwood, G.: 1.5-Dimensional volatility basis set approach for modeling

588   organic   aerosol   in   CAMx   and   CMAQ,   Atmospheric   Environment,   95,   158-164,

589   https://doi.org/10.1016/j.atmosenv.2014.06.031, 2014.

590   Lim, Y. B., and Ziemann, P. J.: Effects of molecular structure on aerosol yields from OH

591   radical-initiated reactions of linear, branched, and cyclic alkanes in the presence of NO x,

592   Environmental science & technology, 43, 2328-2334, 2009.

593   Lu, K., Guo, S., Tan, Z., Wang, H., Shang, D., Liu, Y., Li, X., Wu, Z., Hu, M., and Zhang, Y.: Exploring
594   atmospheric free-radical chemistry in China: the self-cleansing capacity and the formation of secondary
595   air pollution, National Science Review, 6, 579-594, 2019.

596   Lu, Q., Zhao, Y., and Robinson, A. L.: Comprehensive organic emission profiles for gasoline, diesel,
597   and gas-turbine engines including intermediate and semi-volatile organic compound emissions,
598   Atmospheric Chemistry and Physics, 18, 17637-17654, 2018.

599   Ma, R., He, X., Zheng, Y., Zhou, B., Lu, S., and Wu, Y.: Real-world driving cycles and energy
600   consumption informed by large-sized vehicle trajectory data, Journal of Cleaner Production, 223,
601   564-574, https://doi.org/10.1016/j.jclepro.2019.03.002, 2019.

602   Marotta, A., Pavlovic, J., Ciuffo, B., Serra, S., and Fontaras, G.: Gaseous Emissions from Light-Duty
603   Vehicles: Moving from NEDC to the New WLTP Test Procedure, Environmental Science &
604   Technology, 49, 8315-8322, 10.1021/acs.est.5b01364, 2015.

605   May, A. A., Nguyen, N. T., Presto, A. A., Gordon, T. D., Lipsky, E. M., Karve, M., Gutierrez, A.,
606   Robertson, W. H., Zhang, M., Brandow, C., Chang, O., Chen, S. Y., Cicero-Fernandez, P., Dinkins, L.,
607   Fuentes, M., Huang, S. M., Ling, R., Long, J., Maddox, C., Massetti, J., McCauley, E., Miguel, A., Na,
608   K., Ong, R., Pang, Y. B., Rieger, P., Sax, T., Truong, T., Vo, T., Chattopadhyay, S., Maldonado, H.,
609   Maricq, M. M., and Robinson, A. L.: Gas- and particle-phase primary emissions from in-use, on-road
610   gasoline and diesel vehicles, Atmospheric Environment, 88, 247-260, 2014.

611   Murphy, B. N., Woody, M. C., Jimenez, J. L., Carlton, A. M. G., and Pye, H. O. T.: Semivolatile POA
612   and parameterized total combustion SOA in CMAQv5.2: impacts on source strength and partitioning,
613   Atmospheric Chemistry & Physics, 17, 11107-11133, 2017.

614   Ng, N., Kroll, J., Chan, A., Chhabra, P., Flagan, R., and Seinfeld, J.: Secondary organic aerosol
615   formation from m-xylene, toluene, and benzene, Atmospheric Chemistry and Physics, 7, 3909-3922,
616   2007.

617   Peng, J. F., Hu, M., Du, Z. F., Wang, Y. H., Zheng, J., Zhang, W. B., Yang, Y. D., Qin, Y. H., Zheng, R.,
618   Xiao, Y., Wu, Y. S., Lu, S. H., Wu, Z. J., Guo, S., Mao, H. J., and Shuai, S. J.: Gasoline aromatics: a
619   critical determinant of urban secondary organic aerosol formation, Atmospheric Chemistry and Physics,
620   17, 10743-10752, 10.5194/acp-17-10743-2017, 2017.

621   Presto, A. A., Miracolo, M. A., Donahue, N. M., and Robinson, A. L.: Secondary organic aerosol
622   formation from high-NO(x) photo-oxidation of low volatility precursors: n-alkanes, Environmental
623   Science & Technology, 44, 2029-2034, 2010.

624   Pretsch, E., Clerc, T., Seibl, J., and Simon, W.: Tables of spectral data for structure determination of
625   organic compounds, Springer Science & Business Media, 2013.

626   Qi, L., Liu, H., Shen, X. e., Fu, M., Huang, F., Man, H., Deng, F., Shaikh, A. A., Wang, X., Dong, R.,
627   Song, C., and He, K.: Intermediate-Volatility Organic Compound Emissions from Nonroad
628   Construction Machinery under Different Operation Modes, Environmental Science & Technology, 53,
629   13832-13840, 10.1021/acs.est.9b01316, 2019.

630   Robinson, A. L., Donahue, N. M., Shrivastava, M. K., Weitkamp, E. A., Sage, A. M., Grieshop, A. P.,
631   Lane, T. E., Pierce, J. R., and Pandis, S. N.: Rethinking Organic Aerosols: Semivolatile Emissions and
632   Photochemical Aging, Science, 315, 1259-1262, 2007.

633   Saliba, G., Saleh, R., Zhao, Y., Presto, A. A., Larnbe, A. T., Frodin, B., Sardar, S., Maldonado, H.,
634   Maddox, C., May, A. A., Drozd, G. T., Goldstein, A. H., Russell, L. M., Hagen, F., and Robinson, A. L.:
635   Comparison of Gasoline Direct-Injection (GDI) and Port Fuel Injection (PFI) Vehicle Emissions:

636   Emission Certification Standards, Cold-Start, Secondary Organic Aerosol Formation Potential, and

637   Potential Climate Impacts, Environmental Science & Technology, 51, 6542-6552,

638   10.1021/acs.est.6b06509, 2017.

639   Spencer, M. T., Shields, L. G., Sodeman, D. A., Toner, S. M., and Prather, K. A.: Comparison of oil and

640   fuel particle chemical signatures with particle emissions from heavy and light duty vehicles,

641   Atmospheric Environment, 40, 5224-5235, 2006.

642   Suarez-Bertoa, R., Zardini, A. A., Keuken, H., and Astorga, C.: Impact of ethanol containing gasoline

643   blends on emissions from a flex-fuel vehicle tested over the Worldwide Harmonized Light duty Test

644   Cycle (WLTC), Fuel, 143, 173-182, https://doi.org/10.1016/j.fuel.2014.10.076, 2015.

645   Tang, R., Wu, Z., Li, X., Wang, Y., Shang, D., Xiao, Y., Li, M., Zeng, L., Wu, Z., Hallquist, M., Hu, M.,

646   and Guo, S.: Primary and secondary organic aerosols in summer 2016 in Beijing, Atmos. Chem. Phys.,

647   18, 4055-4068, 10.5194/acp-18-4055-2018, 2018.

648   Tang, R., Wang, H., Liu, Y., and Guo, S.: Constituents of Atmospheric Semi-Volatile and Intermediate

649   Volatility Organic Compounds and Their Contribution to Organic Aerosol, PROGRESS IN

650   CHEMISTRY, 31, 180-190, 2019.

651   Woody, M. C., Wong, H. W., West, J. J., and Arunachalam, S.: Multiscale predictions of

652   aviation-attributable PM2.5 for US airports modeled using CMAQ with plume-in-grid and an

653   aircraft-specific 1-D emission model, Atmospheric Environment, 147, 384-394,

654   10.1016/j.atmosenv.2016.10.016, 2016.

655   Yuan, B., Hu, W. W., Shao, M., Wang, M., Chen, W. T., Lu, S. H., Zeng, L. M., and Hu, M.: VOC

656   emissions, evolutions and contributions to SOA formation at a receptor site in eastern China,

657   Atmospheric Chemistry and Physics, 13, 8815-8832, 10.5194/acp-13-8815-2013, 2013.

658   Zhang, Q., Jimenez, J., Canagaratna, M., Allan, J., Coe, H., Ulbrich, I., Alfarra, M., Takami, A.,

659   Middlebrook, A., and Sun, Y.: Ubiquity and dominance of oxygenated species in organic aerosols in

660   anthropogenically‐influenced Northern Hemisphere midlatitudes, Geophysical Research Letters, 34,

661   2007.

662   Zhao, Y., Hennigan, C. J., May, A. A., Tkacik, D. S., de Gouw, J. A., Gilman, J. B., Kuster, W. C.,

663   Borbon, A., and Robinson, A. L.: Intermediate-Volatility Organic Compounds: A Large Source of

664   Secondary Organic Aerosol, Environmental Science & Technology, 48, 13743-13750,

665   10.1021/es5035188, 2014.

666   Zhao, Y., Nguyen, N. T., Presto, A. A., Hennigan, C. J., May, A. A., and Robinson, A. L.: Intermediate

667   Volatility Organic Compound Emissions from On-Road Diesel Vehicles: Chemical Composition,

668   Emission Factors, and Estimated Secondary Organic Aerosol Production, Environmental Science &

669   Technology, 49, 11516-11526, 10.1021/acs.est.3b02841, 2015.

670   Zhao, Y., Nguyen, N. T., Presto, A. A., Hennigan, C. J., May, A. A., and Robinson, A. L.: Intermediate

671   Volatility Organic Compound Emissions from On-Road Gasoline Vehicles and Small Off-Road

672   Gasoline Engines, Environmental Science & Technology, 50, 4554-4563, 10.1021/acs.est.5b06247,

673   2016.

674   Zhao, Y., Lambe, A. T., Saleh, R., Saliba, G., and Robinson, A. L.: Secondary organic aerosol

675   production from gasoline vehicle exhaust: Effects of engine technology, cold start, and emission

676   certification standard, Environmental science & technology, 52, 1253-1261, 2018.

677

678

679 **Figure Caption**

680 **Figure 1.** IVOC emission factors measured under different conditions, i.e. different

681 fuel type (gasoline, E10), test cycles (Chinese Light vehicles Test Cycle, CLTC,

682 and World-wide harmonized Light-duty Test Cycle, WLTC), starting mode (hot

683 start and cold start), and acceleration rates (acceleration rates of 1.2, 3.6 and 6.0

684 km/h/s). Stars indicate the EF data from US, i.e. median US LEV-2 gasoline

685 vehicles (vehicles manufactured in 2004-2012), non-road construction machinery,

686 and a large cargo vessel (Qi et al., 2019;Huang et al., 2018;Zhao et al., 2016). The

687 first category "China V" is the compilation of all the EF results from all of the

688 CLTC and WLTC tests. The boxes indicate the median value, with error bars

689 represent one standard deviation.

690 **Figure 2.** (a) Comparison of average chemical speciation of IVOC emissions from

691 China V vehicle and US vehicles (Zhao et al., 2016); (b) Average mass spectrum

692 of the IVOC during a typical E10-fueled cold start CLTC test. (c-d) Box-whisker

693 plots of the fractional contribution of selected fragments to total IVOCs signal for

694 tested China V vehicle:(c) B_{12}-B_{16} bins; (d) B_{17}-B_{22} bins. The boxes represent the

695 25th and 75th percentiles with the centerline being the median. The whiskers are the

696 10th and 90th percentiles. Black hollow triangles represent median LEV-2 data

697 from Zhao et al. [13] LEV-2 represents vehicles manufactured from 2004 to 2012.

698 Fragments colored in blue represent aliphatic compounds, while those colored in

699 orange are associated with aromatic compounds.

700 **Figure 3.** Comparison of IVOC volatility distributions of Chinses gasoline vehicle

701 exhaust, US gasoline vehicle exhaust, and Chinses E10 fuel. The box-plot

702 represents the Chinses gasoline vehicle exhaust. The boxes represent the 25th and

703 75th percentiles with the centerline being the median. The whiskers are the 10th and

704 90th percentiles. Red solid circles and blue hollow triangle represent IVOC

705 fractions of US vehicle exhaust (Zhao et al., 2016) and Chinese E10 fuel in

706 different volatility bins, respectively.

707 **Figure 4.** Comparison of emission factors of (a) PM (b) NO_x (c) THC, and (d) IVOC

708 between China and US on road gasoline vehicles (Zhao et al., 2016;May et al.,

709 2014). The boxes present the 75th and 25th percentiles with the centerline

710 represents being the median. The US vehicles are grouped by the model year, i.e.

711 pre-LEV refers to vehicles manufactured prior to 1994, LEV-1 represents vehicles

712 from 1994-2003, and LEV-2 is vehicles manufactured from 2004-2012.

713 **Figure 5** Comparison of POA and estimated SOA production after 48 h of

714 photo-oxidation (a) under low NO_x condition; (b) at an OA loading of 10 $\mu g \cdot m^{-3}$

715 under high NO_x condition; (c) at an OA loading of 20 $\mu g \cdot m^{-3}$ under high NO_x

716 condition; (d) at an OA loading of 80 $\mu g \cdot m^{-3}$ under high NO_x condition.

717
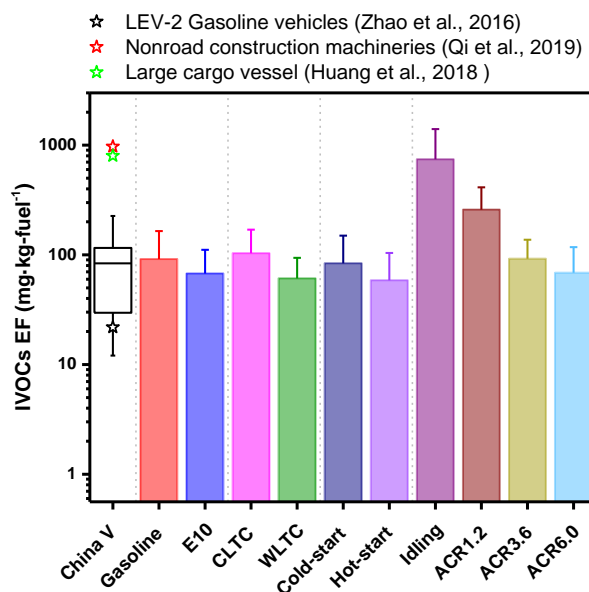
Figure 1. IVOC emission factors measured under different conditions, i.e. different fuel type (gasoline, E10), test cycles (Chinese Light vehicles Test Cycle, CLTC, and World-wide harmonized Light-duty Test Cycle, WLTC), starting mode (hot start and cold start), and acceleration rates (acceleration rates of 1.2, 3.6 and 6.0 km/h/s). Stars indicate the EF data from US, i.e. median US LEV-2 gasoline vehicles (vehicles manufactured in 2004-2012), non-road construction machinery, and a large cargo vessel (Qi et al., 2019;Huang et al., 2018;Zhao et al., 2016). The first category "China V" is the compilation of all the EF results from all of the CLTC and WLTC tests. The boxes indicate the median value, with error bars represent one standard deviation.
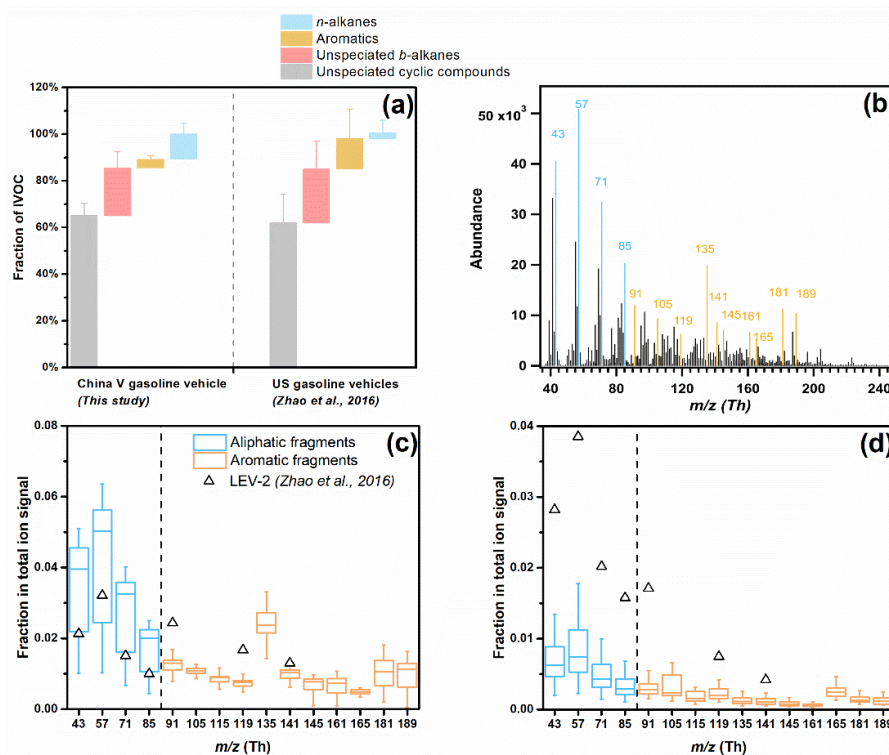
728

Figure 2. (a) Comparison of average chemical speciation of IVOC emissions from China V vehicle and US vehicles (Zhao et al., 2016); (b) Average mass spectrum of the IVOC during a typical E10-fueled cold start CLTC test. (c-d) Box-whisker plots of the fractional contribution of selected fragments to total IVOCs signal for tested China V vehicle:(c) B_{12}-B_{16} bins; (d) B_{17}-B_{22} bins. The boxes represent the 25th and 75th percentiles with the centerline being the median. The whiskers are the 10th and 90th percentiles. Black hollow triangles represent median LEV-2 data from Zhao et al. (2016) LEV-2 represents vehicles manufactured from 2004 to 2012. Fragments colored in blue represent aliphatic compounds, while those colored in orange are associated with aromatic compounds.

739
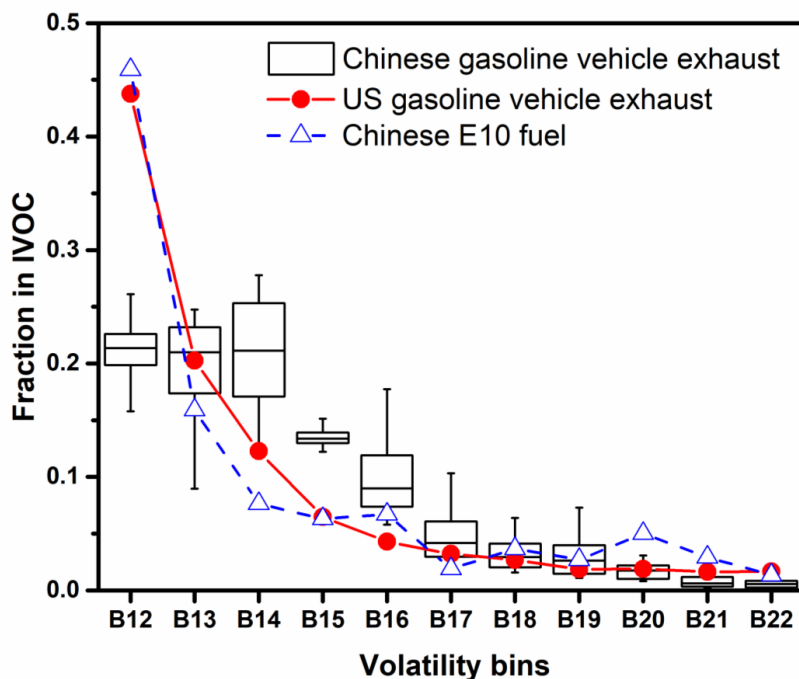
740

Figure 3. Comparison of IVOC volatility distributions of Chinses gasoline vehicle

exhaust, US gasoline vehicle exhaust, and Chinses E10 fuel. The box-plot represents

the Chinses gasoline vehicle exhaust. The boxes represent the 25th and 75th percentiles

with the centerline being the median. The whiskers are the 10th and 90th percentiles.

Red solid circles and blue hollow triangle represent IVOC fractions of US vehicle

exhaust (Zhao et al., 2016) and Chinese E10 fuel in different volatility bins,
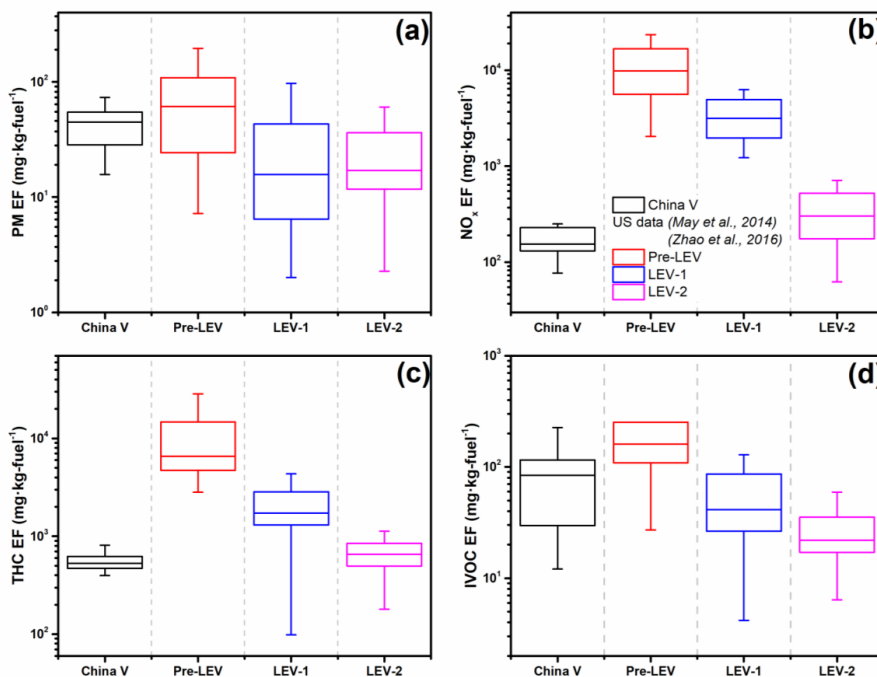
respectively.

748

749

Figure 4. Comparison of emission factors of (a) PM (b) NO$_x$ (c) THC, and (d) IVOC

between China and US on road gasoline vehicles (Zhao et al., 2016;May et al., 2014).

The boxes present the 75th and 25th percentiles with the centerline represents being the

median. The US vehicles are grouped by the model year, i.e. pre-LEV refers to

vehicles manufactured prior to 1994, LEV-1 represents vehicles from 1994-2003, and

LEV-2 is vehicles manufactured from 2004-2012.

756
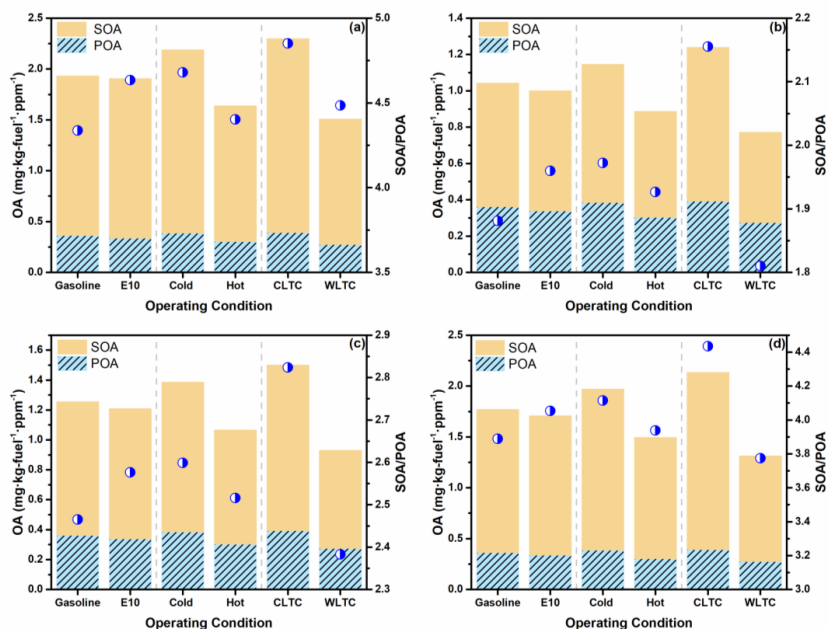
757

Figure 5 Comparison of POA and estimated SOA production after 48 h of photo-oxidation (a) under low NO_x condition; (b) at an OA loading of 10 $\mu g \cdot m^{-3}$ under high NO_x condition; (c) at an OA loading of 20 $\mu g \cdot m^{-3}$ under high NO_x condition; (d) at an OA loading of 80 $\mu g \cdot m^{-3}$ under high NO_x condition.

762

763

764